ACS APPLIED MATERIALS & INTERFACES

Research Article

www.acsami.org

Layer-by-Layer Assembly of Multifunctional Porous N-Doped Carbon Nanotube Hybrid Architectures for Flexible Conductors and Beyond

Songfang Zhao,[†,‡] Yongju Gao,[†,§] Jinhui Li,[†,‡] Guoping Zhang,*[,†,∥] Chunyi Zhi,[⊥] Libo Deng,[†] Rong Sun,*[,†] and Ching-Ping Wong[∥]

[†]Shenzhen Institutes of Advanced Technology and [‡]Shenzhen College of Advanced Technology, University of Chinese Academy of Sciences, Shenzhen 518055, China

[§]Nano Science and Technology Institute, University of Science and Technology of China (USTC), Suzhou 215123, China

[∥]School of Materials Science and Engineering, Georgia Institute of Technology, 771 Ferst Drive, Atlanta, Georgia 30332, United States

[⊥]Department of Physics and Materials Science, City University of Hong Kong, Hong Kong, China

Supporting Information

ABSTRACT: Coassemble diverse functional nanomaterials with carbon nanotubes (CNTs) to form three-dimensional (3D) porous CNTs hybrid architectures (CHAs) are potentially desirable for applications in energy storage, flexible conductors, and catalysis, because of diverse functionalities and synergistic effects in the CHAs. Herein, we report a scalable strategy to incorporate various functional nanomaterials with N-doped CNTs (N-CNTs) into such 3D porous CHAs on the polyurethane (PU) sponge skeletons via layer-by-layer (LbL) assembly. To investigate their properties and applications, the specific CHAs based on N-CNTs and Ag nanoparticles (NPs), denoted as PU-(N-CNTs/Ag NPs)$_n$, are developed. The unique binary structure enables these specific CHAs conductors to possess reliable mechanical and electrical performance under various elastic deformations as well as excellent hydrophilicity. Moreover, they are employed as strain-gauge sensor and heterogeneous catalyst, respectively. The sensor could detect continuous signal, static signal, and pulse signal with superior sustainability and reversibility, indicating an important branch of electromechanical devices. Furthermore, the synergistic effects among N-CNTs, Ag NPs, and porous structure endow the CHAs with excellent performance in catalysis. We have a great expectation that LbL assembly can afford a universal route for incorporating diverse functional materials into one structure.

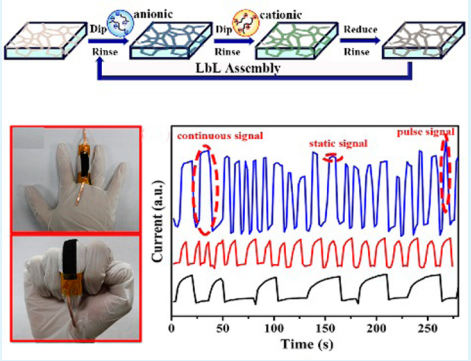

KEYWORDS: *layer-by-layer assembly, flexible conductor, strain-gauge sensor, heterogeneous catalysis, man−machine interaction*

1. INTRODUCTION

Elastic conductors and electric circuits, which retain high conductivity of interconnects under substantial degrees of bending, shearing, twisting, and compression deformation, are highly desirable for applications in flexible displays, energy-related devices, deformable antenna and capacitors, smart clothing, and actuators.[1−5] To address the conductivity−flexibility dilemma, a large number of conductively flexible materials have been developed, such as conductive thin films configured into waves or buckles on flexible substrates,[6−9] carbon nanotubes (CNTs) and metal nanowires coated on stretchable fabrics,[10,11] conductive fillers embedded in composite elastomers,[12−14] and three-dimensional (3D) conductive composite materials.[15−17] A promising approach for a flexible conductor/sensor is developing conductive interconnected 3D structural materials by a facile assembly method. In particular, carbon nanotubes have gained much attention as distinctive nanoscale building blocks to construct novel 3D porous architectures, due to their high aspect ratio, excellent electrical conductivity, and mechanical robustness. These 3D architectures exhibit high specific surface area as well as a fast transport channel of charge carriers.[18−21] More importantly, one critical step in extending their specific applications is how to incorporate a diverse functional component into such porous CNTs structures to form multifunctional porous CNTs hybrid architectures (CHAs), because of diverse functionalities and synergistic effects in CHAs. Several approaches,[22−24] such as chemical vapor deposition (CVD), hydrothermal coassembly, and template-assisted growth, have been developed to assemble such 3D porous CHAs. However, there are three main challenges which render further development of 3D porous CHAs substantially difficult. The first one lies in the difficulty in controlling the thickness and multiple layers of various functional materials on

Received: January 6, 2015
Accepted: March 6, 2015
Published: March 6, 2015

DOI: 10.1021/acsami.5b00116
ACS Appl. Mater. Interfaces 2015, 7, 6716−6723

nonregular geometric surfaces. The second one is the lack of multifunctional diversity of CHAs, due to the immiscibility and incompatibility of nanomaterials with CNTs by solution-based approach. Moreover, these methods require highly time- and energy-consuming cryodesiccation or CVD procedures,[22] impeding the large-scale production of CHAs. To address these challenges, it is highly desirable to develop a simple and scalable method to assemble functional materials with CNTs to form 3D porous CHAs for diverse applications.

Layer-by-layer (LbL) assembly is a versatile and simple method to fabricate multifunctional, multilayer thin films on the surface, which involves the repeated, sequential immersion of substrates into desired solution.[25−27] Here, we report a simple and rapid method to incorporate diverse functional nanomaterials into 3D porous CHAs for flexible conductors on the basis of commercially available polyurethane (PU) sponge and LbL assembly. The key novelty to assemble such binary CHAs lies in selection of available PU sponges with macroscopically ordered 3D structure as the skeleton and synthesis of novel polyelectrolyte as surfactant and adhesion layer for immobilizing various nanostructured materials. Moreover, the facile LbL assembly is environmentally friendly and easily scaled up, making practical application of the resultant 3D porous CHAs possible. As a proof of concept, the specific CHAs based on N-doped CNTs (N-CNTs) and Ag nanoparticles (NPs), denoted as PU-(N-CNTs/Ag NPs)$_n$, are successfully assembled and their applications for strain-gauge sensor and heterogeneous catalysts are demonstrated in detail, which show excellent performance due to the synergistic effects among N-CNTs, Ag NPs, and porous structure.

2. MATERIALS AND METHODS

2.1. Materials. Methylene bis(acrylamide) (MBA) and 1-(2-aminoethyl) piperazine (AEPZ) were purchased from Aldrich Reagent Co., Ltd. L-Ascorbic acid (LAA) and alginate were purchased from Aladdin Reagent Co., Ltd. Methylene blue (MB, $C_{16}H_{18}ClN_3S$), *p*-nitrophenol (4-NP, $C_6H_5NO_3$), rhidamine B (RhB, $C_{28}H_{31}ClN_2O_3$), orange G (OG, $C_{16}H_{10}N_2Na_2O_7S_2$), and sodium borohydride were purchased from Sinopharm Chemical Reagent Co., Ltd. N-CNTs was purchased from Chengdu Chemicals Co. Ltd. (China), and its diameter is 30−50 nm with a length of 10−30 μm, and its purity is above 95% with a N content of 2.98 wt %.

2.2. Synthesis of Hyperbranched Polyamidoamine (HPAM). HPAM was synthesized via conventional Michael addition polymerization (Figure S1, Supporting Information).[28,29] A typical polymerization procedure was as follows: MBA (616 mg, 4 mmol) was added into a solution of AEPZ (516 mg, 4 mmol) in a 10 mL solvent mixture (methanol/water, 70/30, V/V). After complete mixing, polymerization is carried out at 50 °C for 144 h. It is to be noted that the sequence of adding monomers could affect the solubility of HPAM. The product was dissolved in methanol and then precipitated in acetone. This process was repeated at least three times. The dry polymer was then obtained by freeze drying. The disappearance of the proton signal in ethylene of MBA at 5.6 and 6.2 ppm indicates completion of polymerization (Figure S2, Supporting Information).

2.3. Fabrication of CHAs by LbL Assembly. On the day of coating, macroporous PU sponges were cleaned by deionized water and ethanol several times, followed by completely drying at 80 °C for 2 h. PU sponges were then alternatively dipped into the anionic and cationic polyelectrolyte. Initial dips retain for 5 min each, while subsequent dips were 1 min. Foams were squeezed by hand to expel liquid, gently dried with compressed air, rinsed with deionized water for 1 min, and gently dried with compressed air again. In the case of cationic polyelectrolyte-containing metal ions, a procedure of dipping sponges in LAA solution was added after deposition of the HPAM layer. A typical procedure of fabricating PU-(N-CNTs/Ag NPs)$_n$ architectures is shown in Figure 1a in detail. Cationic polyelectrolyte was prepared by mixing HPAM aqueous solution (0.4%) with the same amount of $AgNO_3$ aqueous solution (50 mg mL^{-1}), while anionic polyelectrolyte was prepared by mixing alginate aqueous solution (0.4%) with the same amount of oxide N-CNTs aqueous solution (6 mg mL^{-1}), which was obtained according to our previous work.[30] First, cleaned PU sponges are dipped into anionic solution for 5 min. Second, the resultant sponges were submerged into cationic polyelectrolyte for 1 min. Lastly, the absorbed silver ions were in situ reduced into Ag NPs by LAA solution. All sponges in each procedure experience squeezing, rinsing, and drying. After the desired numbers of bilayers were deposited via the above procedures, CHAs were completely dried before testing.

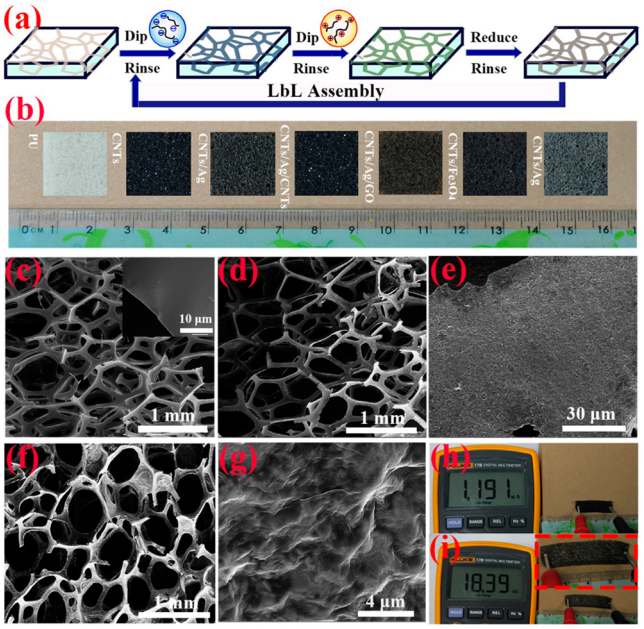

Figure 1. (a) Schematic procedure for the fabrication of porous CHAs by layer-by-layer assembly. (b) Optical images of PU and CHAs. (c) SEM images of PU. (d, e) SEM images of PU-(N-CNTs) architecture. (f, g) SEM images of PU-(N-CNTs/Ag NPs/GO) hybrid architectures. (h, i) Electric resistance of PU-(N-CNTs/Ag NPs)$_n$ fabricated by LbL assembly. (h) n = 1.5, (i) n = 5.

2.4. Characterization. The morphology and microstructure were investigated by field-emission scanning electron microscopy (FE-SEM, nanoSEM 450, NOVA, USA). Ultraviolet−visible spectroscopy (UV−vis) absorption spectra of the samples are recorded on an UV−vis−NIR spectrometer (Shimadzu UV-3000) with a wavelength range of 250−800 nm. The X-ray diffraction (XRD) diagrams of the samples were measured on an X-ray diffractometer (Rigaku D/Max 2500) with monochromated Cu Kα radiation (λ = 1.54 Å) at a scanning rate of 8 deg/min^{-1}. The dynamic modulus of CHAs was measured using small amplitude oscillatory shear (0.1%) on an Anton Paar MCR 302 rheometer. ^{1}H NMR and ^{13}C NMR spectra were recorded on a Bruker AV400 NMR spectrometer in deuterated DMSO at room temperature, and the chemical shifts are given in ppm relative to tetramethylsilane as the internal reference. The electrical resistance variation was measured by a two-probe method under various mechanical deformations. During the measurement, two copper sheets serve as electrodes to connect CHAs to a Keithley 2410 Source Meter instrument. Every electromechanical experiment was repeated 3 times, and the value of electrical resistance is the average value. Compressive stress−strain measurements were performed using an electronic universal testing machine (RGM-4000, REGER Co. Ltd., China) with two test plates. The samples were set on the lower plate and compressed by the upper plate connecting to a load cell. The strain ramp rate was controlled to be 2 mm min^{-1} for the measurements.

DOI: 10.1021/acsami.5b00116
ACS Appl. Mater. Interfaces 2015, 7, 6716−6723

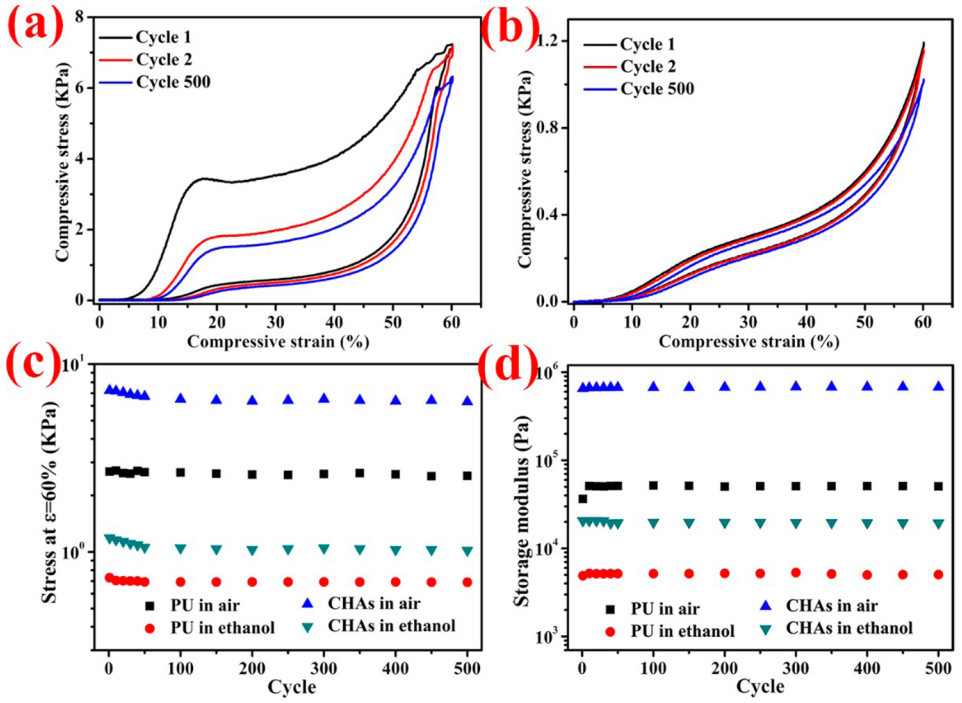

Figure 2. Cyclic compression stress−strain curves of PU-(N-CNTs/Ag NPs)$_{1.5}$ at the compression speed of 2 mm min^{-1} (a) in the dry state and (b) in the wet state (ethanol). (c) Stress recorded at set ε = 60% vs cycles for comparing PU and CHAs in different states, showing an increase of at least ca. 100% in compressive stress. (d) Storage modulus recorded at 10 rad s^{-1} set ε = 60% vs cycles for comparing PU and CHAs in different states, showing no obvious modulus degradation.

The current response of as-prepared strain-gauge sensor iwass recorded using a paperless current monitoring recorder (WZ-2300RX, Lingshuo Testing Equipment Co. Ltd., China).

2.5. Catalytic Performance Tests. The catalytic performance of the prepared CHAs was investigated by measuring the reduction and degradation of various dyes, namely, 4-NP, OG, MB, and RhB, in the presence of $NaBH_4$. In a typical procedure, 5 mL of 4-NP or OG aqueous solution (0.4 mM) was mixed with 10 mL of fresh $NaBH_4$ solution (40 mM). In the case of MB and RhB, 5 mL of MB or RhB aqueous solution was mixed with 10 mL of fresh $NaBH_4$ solution (40 mM) and 25 mL of deionized water. Then 3.5 mL of mixture and 12 mg of CHAs were placed into a quartz cell. The progress of the conversion reaction was monitored by recording the time-dependent UV−vis absorption spectra of the mixture using a spectrophotometer.

3. RESULTS AND DISCUSSION

3.1. CHAs Fabrication via LbL Assembly and Structure Characterization. Figure 1a schematically illustrates the scalable fabrication process of porous CHAs by LbL assembly. In a typical experiment, commercially available, precleaning PU sponges with 3D-interconneted networks are dipped into anionic solution; thus, the bare PU sponges are successfully coated with oxide N-CNTs and alginate, owing to the unique macropores of sponges and repeated squeezing. After rinsing and drying, the sponge color changes from white to black (Figure 1b) and the skeletons of sponge are uniformly coated with the N-CNTs (Figure 1d and 1e), resulting in a conductive sponge with crumpled and rough texture associated with the aggregation of N-CNTs. Then, the N-CNTs-coated PU sponges are immersed into an aqueous solution of $AgNO_3$ and HPAM, which is synthesized by a one-pot Michael addition polymerization (Figures S1 and S2, Supporting Information). After procedures of squeezing, rinsing, and drying, the LAA aqueous solution is injected into the resultant sponges to reduce the absorbed silver ions into Ag NPs. After rinsing and drying, the sponge color changes from black to light gray and the microfibers are decorated by Ag NPs (Figure S1a−c, Supporting Information), resulting in a composite conductive sponge with well-defined nano/microscale network structures. It should be noted that 5 min of initial dip is guaranteed to obtain perfect surface coverage, which allows complete charge reversion of the surface and consecutive growth of the multilayers. To verify the feasibility and scalability of our strategy, several typical nanomaterials, which vary in shapes, size, and preparation methods, are employed to coassemble with N-CNTs to prepare other porous CHAs in Figure 2b, and their structures are characterized by XRD as shown in Figure S4, Supporting Information, indicating the coassembly of diverse nanomaterials (Ag NPs, Fe_3O_4 NPs, etc.) with N-CNTs into one architecture simultaneously. For example, PU-(N-CNTs/Ag NPs/GO) hybrid architecture is also prepared. Figure 1f and 1g illustrates that the skeletons of the network exhibit a wrinkled and rough texture, indicating the assembly of Ag NPs and GO sheets on the struts of the network. After undergoing a subsequent hydrazine hydrate treatment, the reduced GO (rGO) sheets are in situ assembled on the skeletons (Figure S1g−i, Supporting Information), with a color change from yellow to black (Figure 1b), and the resulting CHAs possess good flexibility as well as excellent electrical conductivity.

We should take note that the polyelectrolyte layer plays a critical role in the microstructure and properties of CHAs. It acts not only on the adhesion layer between the multifunctional nanomaterials and the sponges but also on the surfactant to form stable suspension via various interactions. Moreover, the properties of CHAs are dependent on the number of deposited layers. As an example, the electric conductivity of PU-(N-CNTs/Ag NPs)$_n$ is calculated, which is 4.95×10^{-4} and 4.61×10^{-2} S/m for n = 1.5 and 5, respectively (Figure 1h and 1i).

DOI: 10.1021/acsami.5b00116
ACS Appl. Mater. Interfaces 2015, 7, 6716−6723

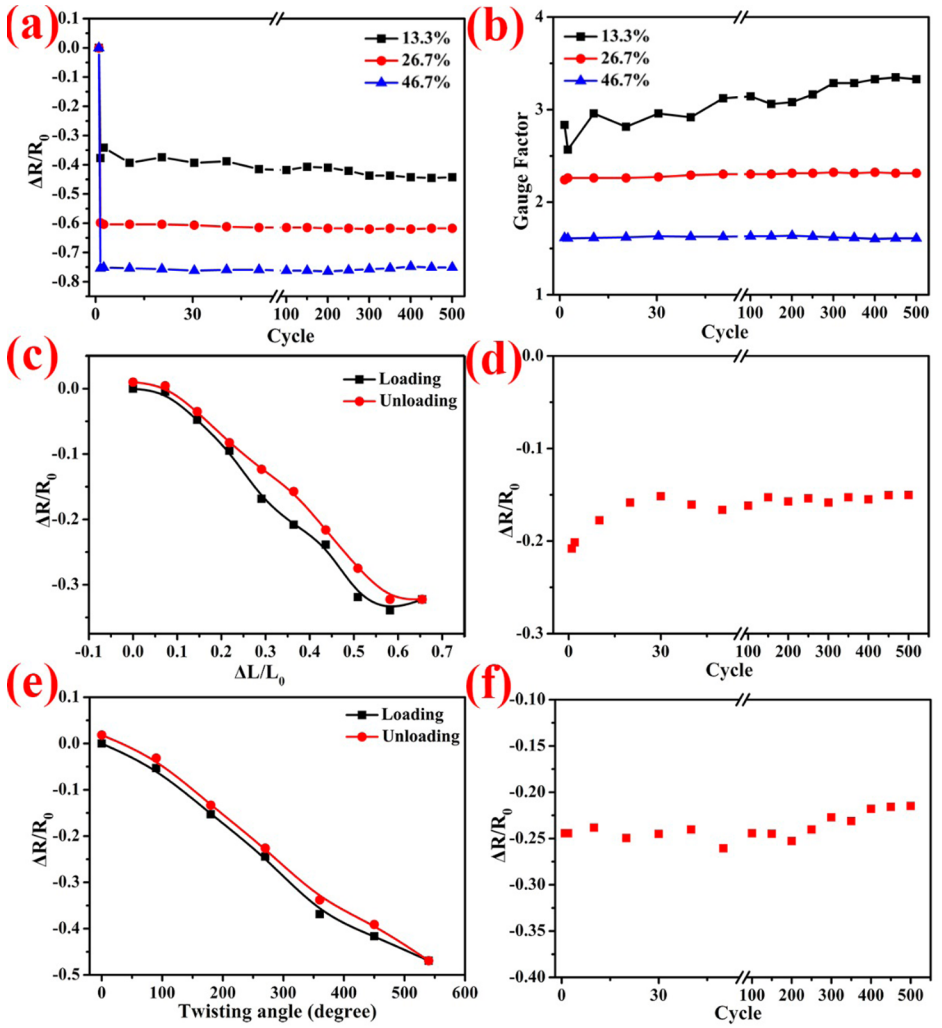

Figure 3. Electric performance evaluations of the elastic PU-(N-CNTs/Ag NPs)$_{1.5}$ conductors. (a) Resistance change ratio ($\Delta R/R_0$) as a function of applied compression strain for each compressing/releasing cycle. (b) GF at different strains for each cycle. (c) Resistance change ratio ($\Delta R/R_0$) as a function of $\Delta L/L_0$ during a loading an and unloading process (bending process). (d) Resistance change ratio ($\Delta R/R_0$) for each cycle ($\Delta L/L_0 = 0.4$). (e) Resistance change ratio ($\Delta R/R_0$) as a function of twisting angle during a loading and an unloading process (twisting process). (f) Resistance change ratio ($\Delta R/R_0$) for each cycle at a twisting angle of 270°.

The conductivity increases as the deposited layer increases, which is attributed to the increase of the conductive materials. Furthermore, the surface energy is also varied with the number of deposited layer. As shown in Figure S5, Supporting Information, the water contact angle of the original PU sponges is about 120.3°, indicating its hydrophobicity, while the PU-(N-CNTs/Ag NPs/N-CNTs) shows a contact angle of 109.3°. Notably, a droplet is completely absorbed by PU-(CNTs/Ag NPs)$_5$, realizing a wettability transformation from hydrophobicity to hydrophilicity.

Importantly, compared to other strategies to design CHAs, such as sol–gel coassembly[23,31] and the CVD method,[22] the whole process of LbL assembly is solution processed at room or mild condition, and it can be readily scaled up. Besides, it can directly coassemble various functional nanomaterials in one CHA without considering the interaction among the nanomaterials. Finally, the sponge is intrinsically flexible and porous; thus, the CHAs prepared by our method possess flexible skeletons and large size pores, which would not only maintain the excellent physical properties but also enhance the mass/electron transport properties in the CHAs. As a consequence, the designed porous architecture would hold great potential as flexible conductors, strain-gauge sensor, and heterogeneous catalysts, due to the combination of porous structure and the synergistic effects between N-CNTs and other functional nanomaterials.

3.2. Mechanical and Rheological Properties. The excellent mechanical behavior is of great importance for CHAs to be applied in various fields. As a proof of concept, PU-(N-CNTs/Ag NPs)$_{1.5}$ is developed. The porous structure presents superior flexibility and can be bent and twisted without structure disruption (Figures S6a and S6b, Supporting Information). Notably, strong adhesion among N-CNTs, other nanomaterials, and PU is confirmed by washing in water showing no visible residual in the solution (Figures S6c and S6d, Supporting Information). PU sponges are selected to be as skeletons of CHAs, because that the PU sponges can undergo large-strain deformations, and resist structural fatigue under cyclic stress conditions, in both air and liquid (ethanol), as shown in Figure S7, Supporting Information. The loading process of the skeletons exhibits three evident deformation domains: a pronounced linear-elastic region for $\varepsilon < 15\%$, a

DOI: 10.1021/acsami.5b00116
ACS Appl. Mater. Interfaces 2015, 7, 6716–6723

relative plateau region for 15% < ε < 38%, and a steep slope region for ε > 38%. Meanwhile, the stress (σ)−strain (ε) curve of the CHAs prepared by LbL assembly is identical to that of the PU, with the exception that the compressive stress (7.2 KPa) at ε = 60% increases nearly 3 times of the values of PU sponge (2.5 KPa) (Figure 2a). This considerable increase in strength can be attributed to the enhancement of the HPAM/alginate alloy and rigid nanofillers incorporated via LbL assembly.[32] The CHAs can be easily compressed to 60% volume reduction at low stress (~7.2 KPa) due to their high porosity and structural flexibility. The hysteresis loops formed by the loading and unloading curves indicate substantial energy dissipation due to friction between flowing air and the sponge skeleton.[33] In addition, cyclic tests show a small plastic deformation, as seen from the gradual shift of the loading and unloading curves in increasing cycles and high compressive stress of 6.4 KPa with no evident strength degradation after 500 cycles (Figure 2c), indicating excellent mechanical robustness.[34]

The CHAs are also characterized mechanically by immersing them completely in a solvent (e.g., ethanol) bath, in which ethanol is extruded out of the CHAs pores during compression and is reabsorbed during unloading and the expansion of CHAs. However, the stress needed to remove ethanol from the CHAs (~1.2 KPa) is quite lower than that required to remove air (~7.2 KPa), indicating that ethanol flow through the interconnected pore is more smooth. In detail, the excellent wetting behavior of ethanol to CHAs and open-pore structure of CHAs enables the ethanol to flow smoothly and are responsible for the less plastic deformation, whereas the cyclic compression in air enhances the plastic deformation of CHAs due to the friction among the skeletons of CHAs. Moreover, the plastic deformation of CHAs originates from the sliding of skeletons, and the resulting sliding could recover easily in ethanol. Interestingly, the CHAs readily recover their original volume by ethanol uptake during the unloading process, even after 500 cycles, and they can maintain a stable compressive stress in each cycle, implying superior resistance to structural fatigue in ethanol.

To further investigate the structure and properties of the CHAs, the rheological behaviors are also characterized. Small-deformation oscillatory measurements (Figure S8, Supporting Information) reveal that the low-frequency plateau indicates their true elasticity, and subsequently storage modulus (E') increases with the increase of angular frequency in both air and liquid conditions, and E' in the dry state is approximately 20 times higher than that in the wet state, due to the lubrication of ethanol during the oscillating process. In detail, the lower E' in ethanol bath indicates that the ethanol absorbed on CHAs is easily driven out of the CHAs pores during oscillation. The CHAs are completely infiltrated by ethanol, leading to a decrease of the friction among the skeletons of CHAs; moreover, the open-pore structure of CHAs enables the ethanol to flow smoothly. These properties are responsible for the nonoccurrence of plastic deformation, whereas the continuous oscillation in air enhances the plastic deformation of CHAs, which increases the contact area among the skeletons to increase the friction. Furthermore, the E' of CHAs is also ~10 times higher than that of PU sponges, due to the enhancement of the HPAM/alginate alloy and rigid nanofillers through LbL assembly. Notably, all sponges can maintain a similar storage modulus at 10 rad s^{-1} and 60% strain in both air and ethanol for each cycle (Figure 2d), indicating structural robustness under oscillation. The highly structural and chemical stability are favorable for their applications over many cycles.

3.3. Electrical Properties and Strain-Gauge Sensor. Importantly, the unique structure of PU-$(CNTs/Ag\ NPs)_{1.5}$ endows them to be highly compressible, bendable, and twistable while maintaining considerable conductivity. Their resistance variations upon compression, bending, and twisting deformations are investigated, where R_0 is the initial resistance of CHAs. For compression tests, the resistance change ratio ($\Delta R/R_0$) as a function of strain (ε) for each cycle is shown in Figure 3a. It can be seen that the electric resistance decreases with the increase of ε, which is attributed to the increase of contact area between the interfaces of the CHAs and the copper electrode and the increase of contact area among the conductive building blocks.[18] In addition, the cyclic stability of the resistance−strain relation is enhanced under larger deformation, i.e., fewer cycles are needed for CHAs to become stable under high strain, which could be explained by the effective restructure of CHAs under higher strain. In terms of gage sensitivity, the gauge factor (GF) of the CHAs is evaluated, as plotted in Figure 3b. It can also be seen that fewer cycles are needed for the GF to stabilize under larger compression strain, and the GF varies from ca. 1.5 to 3 at investigated strain ranges. Especially, the CHAs has a GF of 3.2 at a strain of 13.3%, which originates from the contact resistance mechanism. Moreover, these variations are related to the different variation rate of contact area at different strain during the compression process, resulting in the nonlinearity of resistance variation (ΔR) vs strain variation ($\Delta\varepsilon$), which is consistent with Cheng's observations.[35]

Furthermore, the response behavior of the CHAs conductors to bending and twisting is also investigated. For bending test, the stress-induced resistance changes are reproducible with moderate hysteresis in loading−unloading cycles except for the first loading−unloading cycle (Figure S9, Supporting Information, Figure 3c). The partial breaking of the conductive percolation network may result in different resistance changes in the first loading−unloading cycle.[36] For the following loading−unloading cycles, the resistance changes become consistent. Moreover, the elastic CHAs show high electromechanical stability on increasing the bending cycles and possess small variations of resistance at a fixed bending strain ($\Delta L/L_0$ = 0.4) after 500 cycles, indicating excellent durability. Similar response characteristic is observed in the twisting tests. The resistance decreases during the bend and twist tests originating from the increase of contact area between the conductive materials under mechanical deformations. To demonstrate the flexibility and high conductivity, the electrical behavior of a simple light-emitting diode (LED) circuit integrated using CHAs as interconnects under various elastic deformation is investigated. As expected, the light intensity of the LED with the applied turn-on voltage of 3 V is almost retained without decrease under twistable, bendable, and foldable deformations in Figure S10, Supporting Information, which shows the feasibility for the CHAs as flexible conductors while retaining high conductivity under various mechanical deformation.

As proof-of-concept applications of porous CHAs, a highly elastic strain-gauge sensor capable of detecting human motion is successfully demonstrated. Figure 4a shows the photograph of the finger-sensor demonstrating the bending and stretching states of the fingers. As shown in Figure 4b, when the finger slowly bends toward the palm and then releases repeatedly, the

DOI: 10.1021/acsami.5b00116
ACS Appl. Mater. Interfaces 2015, 7, 6716−6723

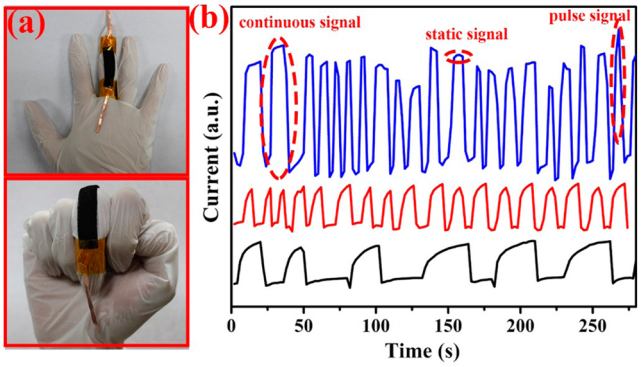

Figure 4. Wearable strain-gauge sensor for detecting finger movement. (a) Photographs of the strain-gauge sensor mounted on the middle figure. The bending (top) and stretching (bottom) states of the finger during testing are also shown. (b) Relative current changes for the strain sensors with different bending speed and bending degree.

finger motion is faithfully recorded by the continuous variation of current. Depending upon the modes of the finger motion, e.g., bending speed, degree, and retaining time, the curves of sensing current variation exhibit different waveforms. For example, the continuous signal, static signal, and pulse signal are generated by manipulating the modes of finger motions, indicating an important branch of electromechanical devices.

3.4. Catalytic Performance of CHAs. As another example, PU-(CNTs/Ag NPs)$_5$ hybrid architectures prepared by LbL assembly are employed as the heterogeneous catalysts to enhance the reduction of various dyes. The catalytic reduction of 4-NP to 4-nitroaniline (4-AP) with an excess amount of $NaBH_4$ is investigated in Figure 5a. The UV−vis absorption spectra of the aqueous mixture of 4-NP and $NaBH_4$ exhibit an extinct absorption peak at 400 nm due to the formation of 4-nitrophenonlate ion in alkaline solution.[37] In the absence of the catalyst, the peak remains unaltered with time, indicating the nonoccurrence of reduction. Upon adding the CHAs, the reduction reaction proceeds, due to the fact that the Ag NPs start the catalytic reduction by relaying electrons from the donor BH_4^- to the acceptor 4-NP (Figure S11, Supporting Information). The reaction progress could be monitored from the time-dependent absorption spectra, which shows the successive decrease of the intensity of the absorption peak at 400 nm, ascribed to nitro compounds, and the concomitant growth of a new peak at 300 nm corresponding to 4-AP, the reduction product of 4-NP (Figure 5a). After completion of the reaction (46 min), the peak at 400 nm is no longer observed, meaning that the catalytic reduction of 4-NP has proceeded successfully. The CHAs can be also employed in other dyes (MB, RhB, and OG) and enhance their reduction and degradation (Figure 4b−d). On the basis of traditional theory on the catalytic reduction of dyes, e.g., 4-NP, by Ag NPs, electron transfer takes place from BH_4^- to 4-NP through adsorption of the reactant molecules onto Ag NPs surfaces, which determines the catalytic performance. In our work, the excellent catalytic performance arises from the synergistic effects of N-CNTs, Ag NPs, and 3D porous structure, explained as follows. (1) CNTs has high adsorption ability toward various dyes containing benzene ring structure via $\pi-\pi$ stacking interactions, which provides a high concentration of dyes near the Ag NPs on CHAs, leading to highly efficient contact between them. (2) When Ag NPs are in contact with semiconductor (N-CNTs), Fermi level alignment occurs, leading to charge redistribution and formation of a depletion layer surrounding the Ag NPs. Thus, electrons leave the Ag NPs into N-CNTs to form an electron-enriched regions, facilitating the uptake of electrons by dyes that happen to be close to these regions. (3) Ag NPs supported on CHAs, which could afford multiple accessible channels for diffusion and

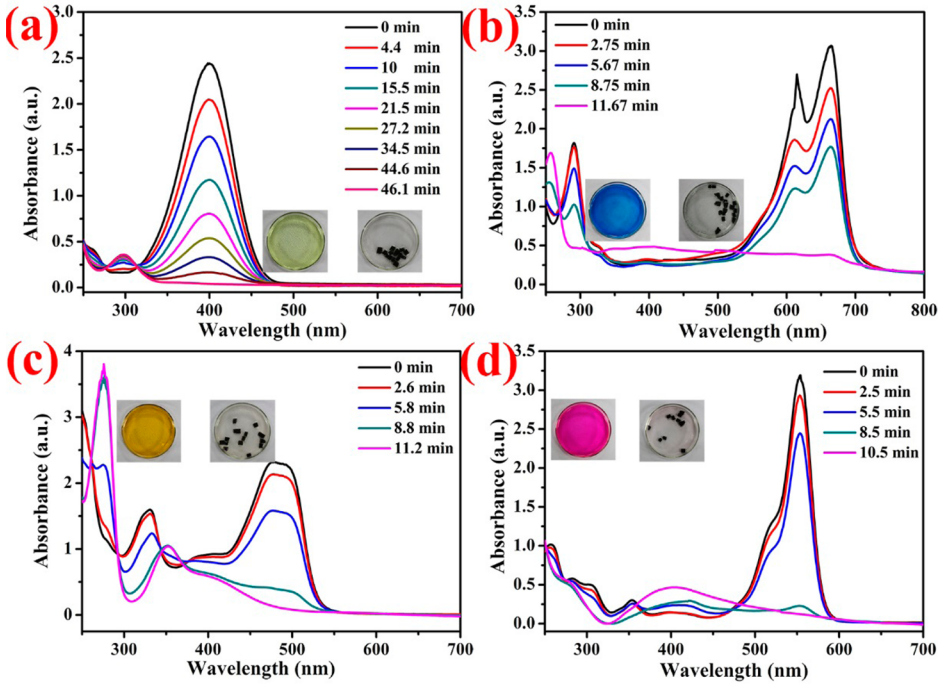

Figure 5. Time-dependent UV−vis absorption spectra during the catalytic reduction of various dyes by PU-(N-CNTs/Ag NPs)$_5$ at room temperature: (a) 4-NP, (b) MB, (c) OG, and (d) RhB.

DOI: 10.1021/acsami.5b00116
ACS Appl. Mater. Interfaces 2015, 7, 6716−6723

transport of the reactant molecules to approach the active sites, enhancing the catalytic performance.[38,39]

4. CONCLUSION

In summary, a layer-by-layer coassembly method, which is scalable and low cost, is developed to prepare binary 3D porous CHAs functionalized by various multifunctional nanomaterials. The key novelty to assemble such binary CHAs lies in selection of available PU sponges with macroscopically ordered 3D structure as the skeletons and synthesis of novel polyelectrolyte as surfactant and adhesion layer for immobilizing various nanostructured materials. Notably, various functional materials with different sizes, shapes, and fabrication methods can be coassembled with N-CNTs into one CHAs with designed functionality. As a proof of concept, the CHAs based on N-CNTs and Ag NPs are successfully assembled. The PU-$(\text{N-CNTs/Ag NPs})_{1.5}$ conductors show reliable mechanical and electrical performance under various elastic deformations. A simple LED demonstration indicates the feasibility of the CHAs conductors in practical application. In addition, the CHAs based on N-CNTs and Ag NPs are employed as strain-gauge sensor and heterogeneous catalyst, respectively, and excellent performance is achieved in both cases. We believe that LbL assembly will open avenues for large-scale production of functional porous materials with desired functionality for applications in flexible conductors, man−machine interaction, heterogeneous catalysis, etc.

■ ASSOCIATED CONTENT

Supporting Information

Additional figures as described in the text; Movie S1. This material is available free of charge via the Internet at http://pubs.acs.org.

■ AUTHOR INFORMATION

Corresponding Authors

*E-mail: gp.zhang@siat.ac.cn.
*E-mail: rong.sun@siat.ac.cn.

Author Contributions

S. Zhao and Y. Gao contributed equally to this work.

Notes

The authors declare no competing financial interest.

■ ACKNOWLEDGMENTS

This work was financially supported by the National Natural Science Foundation of China (Grant No. 21201175), Guangdong and Shenzhen Innovative Research Team Program (No. 2011D052, KYPT20121228160843692), and R&D Funds for basic Research Program of Shenzhen (Grant No. JCYJ20120615140007998).

■ REFERENCES

(1) Kim, Y.; Zhu, J.; Yeom, B. J.; Prima, M. D.; Su, X. L.; Kim, J. G.; Yoo, S. J.; Uher, C.; Kotov, N. A. Stretchable Nanoparticles Conductors with Self-organized Conductive Pathways. *Nature* **2013**, *500*, 59−64.

(2) Yu, Y.; Zeng, J. F.; Chen, C. J.; Xie, Z.; Guo, R. S.; Liu, Z. L.; Zhou, X. C.; Yang, Y.; Zheng, Z. J. Three-Dimensional Compressible and Stretchable Conductive Composites. *Adv. Mater.* **2014**, *26*, 810−815.

(3) Yao, H. B.; Huang, G.; Cui, C. H.; Wang, X. H.; Yu, S. H. Macroscale Elastomeric Conductors Generated from Hydrothermally Synthesized Metal-Polymer Hybrid Nanocable Sponges. *Adv. Mater.* **2011**, *23*, 3643−3647.

(4) Park, M.; Im, J.; Shin, M.; Min, Y.; Park, J.; Cho, H.; Park, S.; Shim, M. B.; Jeon, S.; Chung, D. Y.; Bae, J.; Park, J.; Jeong, U.; Kim, K. Highly Stretchable Electric Circuits from a Composite Material of Silver Nanoparticles and Elastomeric Fibres. *Nat. Nanotechnol.* **2012**, *7*, 803−809.

(5) Lipomi, D. J.; Vosgueritchian, M.; Tee, B. C. K.; Hellstrom, S. L.; Lee, J. A.; Fox, C. H.; Bao, Z. N. Skin-like Pressure and Strain Sensors Based on Transparent Elastic Films of Carbon Nanotubes. *Nat. Nanotechnol.* **2011**, *6*, 788−792.

(6) Yu, C. J.; Masarapu, C.; Rong, J. P.; Wei, B. Q.; Jiang, H. Q. Stretchable Sepercapacitors Based on Buckled Single-Walled Carbon Nanotube Macrofilms. *Adv. Mater.* **2009**, *21*, 4793−4797.

(7) Wang, X. L.; Hu, H.; Shen, Y. D.; Zhou, X. C.; Zheng, Z. J. Stretchable Conductors with Ultrahigh Tensile Strain and Stable Metallic Conductance Enabled by Prestrained Polyelectrolyte Nanoplatforms. *Adv. Mater.* **2011**, *23*, 3090−3094.

(8) Zhu, Y.; Xu, F. Buckling of Aligned Carbon Nanotubes as Stretchable Conductors: A New Manufacturing Strategy. *Adv. Mater.* **2012**, *24*, 1073−1077.

(9) Harris, J. M.; Huh, J. Y.; Semler, M. R.; lhle, T.; Stafford, C. M.; Hudson, S. D.; Fagan, J. A.; Hobble, E. K. Elasticity and Rigidity Percolation in Flexible Carbon Nanotube Films on PDMS Substrates. *Soft Mater.* **2013**, *9*, 11568−11575.

(10) Shin, M.; Song, J. H.; Lim, G. H.; Lim, B.; Park, J. J.; Jeong, U. Highly Stretchable Polymer Transistors Consisting Entirely of Stretchable Device Components. *Adv. Mater.* **2014**, *26*, 3706−3711.

(11) Amjiadi, M.; Pichitpajongkit, A.; Lee, S. J.; Ryu, S.; Park, I. Highly Stretchable and Sensitive Strain Sensor Based on Silver Nanowire-Elastomer Nanocomposite. *ACS Nano* **2014**, *8*, 5154−5163.

(12) Xu, F.; Zhu, Y. Highly Conductive and Stretchable Silver Nanowire Conductors. *Adv. Mater.* **2012**, *24*, 5117−5122.

(13) Yan, C. Y.; Wang, J. X.; Kang, W. B.; Cui, M. Q.; Wang, X.; Foo, C. Y.; Chee, K. J.; Lee, P. S. Highly Stretchable Piezoresistive Graphene-Nanocellulose Nanopaper for Strain Sensors. *Adv. Mater.* **2014**, *26*, 2022−2027.

(14) Zhang, Y. Y.; Sheehan, C. J.; Zhai, J. Y.; Zou, G. F.; Luo, H. M.; Xiong, J.; Zhu, Y. T.; Jia, Q. X. Polymer-Embedded Carbon Nanotube Ribbons for Stretchable Conductors. *Adv. Mater.* **2010**, *22*, 3027−3031.

(15) Yu, Y.; Zeng, J. F.; Chen, C. J.; Xie, Z.; Guo, R. S.; Liu, Z. L.; Zhou, X. C.; Yang, Y.; Zheng, Z. J. Three-Dimensional Compressible and Stretchable Conductive Composites. *Adv. Mater.* **2014**, *26*, 810−815.

(16) Ge, J.; Yao, H. B.; Wang, X.; Ye, Y. D.; Wang, J. L.; Wu, Z. Y.; Liu, J. W.; Fan, F. J.; Gao, H. L.; Zhang, C. L.; Yu, S. H. Stretchable Conductors Based on Silver Nanowires: Improved Performance through a Binary Network Design. *Angew. Chem., Int. Ed.* **2013**, *52*, 1654−1659.

(17) Wu, C.; Huang, X. Y.; Wu, X. F.; Qian, R.; Jiang, P. K. Mechanically Flexible and Multifunctional Polymer-Based Graphene Foams for Elastic Conductors and Oil-Water Separators. *Adv. Mater.* **2013**, *25*, 5658−5662.

(18) Zhao, S. F.; Zhang, G. P.; Gao, Y. J.; Deng, L. B.; Li, J. H.; Sun, R.; Wong, C. P. Strain-Driven and Ultrasensitive Resistive Sensor/Switch Based on Conductive Alginate/Nitrogen-doped Carbon Nanotube-Supported Ag Hybrid Aerogels with Pyramid Design. *ACS Appl. Mater. Interfaces.* **2014**, *6*, 22823−22829.

(19) Zhu, L. B.; Sun, Y. Y.; Hess, D. W.; Wong, C. P. Well-Aligned Open-End Carbon Nanotube Architectures: an Approach for Device Assembly. *Nano Lett.* **2006**, *6*, 243−247.

(20) Tang, C. Y.; Long, G. C.; Hu, X.; Wong, K. W.; Lau, W. M.; Fan, M. K.; Mei, J.; Xu, T.; Wang, B.; Hui, D. Conductive Polymer Nanocomposites with Hierarchical Multi-Scale Structures via Self-assembly of Carbon-Nanotubes on Graphene on Polymer-Microspheres. *NanoScale* **2014**, *6*, 7877−7888.

(21) Shin, U. H.; Jeong, D. W.; Park, S. M.; Kim, S. H.; Lee, H. W.; Kim, J. M. Highly Stretchable Conductors and Piezocapacitive Strain

DOI: 10.1021/acsami.5b00116
ACS Appl. Mater. Interfaces 2015, 7, 6716−6723

Gauges Based on Simple Contact-Transfer Patterning of Carbon Nanotube Forests. *Carbon* **2014**, *80*, 396−404.
(22) Kim, K. H.; Oh, Y.; Islam, M. F. Graphene Coating Makes Carbon Nanotube Aerogels Superelastic and Resistant to Fatigue. *Nat. Nanotechnol.* **2012**, *7*, 562−566.
(23) Niu, Z. Q.; Liu, L. L.; Zhang, L.; Shao, Q.; Zhou, W. Y.; Chen, X. D.; Xie, S. S. A Universal Strategy to Prepare Functional Porous Graphene Hybrid Architectures. *Adv. Mater.* **2014**, *26*, 3681−3687.
(24) Sun, H. Y.; Xu, Z.; Gao, C. Multifunctional, Ultra-Flyweight, Synergistically Assembled Carbon Aerogels. *Adv. Mater.* **2013**, *25*, 2554−2560.
(25) Laufer, G.; Kirkland, C.; Morgan, A. B.; Grunlan, J. C. Exceptionally Flame Retardant Sulfur-Based Multilayer Nanocoating for Polyurethane Prepared from Aqueous Polyelectrolyte Solutions. *ACS Macro Lett.* **2013**, *2*, 361−365.
(26) Hwang, H.; Joo, P.; Kang, M. S.; Ahn, G.; Han, J. T.; Kim, B. S.; Cho, J. H. Highly Tunale Charge Transport in Layer-by-Layer Assembled Graphene Transistors. *ACS Nano* **2012**, *6*, 2432−2440.
(27) Wu, S. Q.; Garfield, L. B.; Rupert, N. E.; Grady, B. P.; Funkhouser, G. P. Strength Improvement via Coating of a Cylindrical Hole by Layer-by-Layer Assembled Polymer Particles. *ACS Appl. Mater. Interfaces* **2010**, *2*, 1220−1227.
(28) Wang, D.; Liu, Y.; Hu, Z. C.; Hong, C. Y.; Pan, C. Y. Michael Addition Polymerizations of Trifunctional Amines with Diacrylamides. *Polymer* **2005**, *46*, 3507−3514.
(29) Wu, D. C.; Liu, Y.; He, C. B.; Chung, T. S.; Goh, S. Effects of Chemistries of Trifunctional Amines on Mechanisms of Michael Addition Polymerizations with Diacrylates. *Macromolecules* **2004**, *37*, 6763−6770.
(30) Zhao, S. F.; Gao, Y. J.; Zhang, G. P.; Deng, L. B.; Li, J. H.; Sun, R.; Wong, C. P. Covalently bonded nitrogen-doped carbon-nanotube-supported Ag hybrid sponges: synthesis, structure manipulation, and its application for flexible conductors and strain-gauge sensors. *Carbon* **2015**, *86*, 225−234.
(31) Tang, Z. H.; Shen, S. L.; Zhuang, J.; Wang, X. Noble-Metal-Promoted Three-Dimensional Macroassembly of Single-layer Graphene Oxide. *Angew. Chem., Int. Ed.* **2010**, *49*, 4603−4607.
(32) Hamedi, M.; Karabulut, E.; Marais, A.; Herland, A.; Nystrom, G.; Wagberg, L. Nanocellulose Aerogels Functionalized by Rapid Layer-by-Layer Assembly for High Charge Storage and Beyond. *Angew. Chem., Int. Ed.* **2013**, *52*, 12038−12042.
(33) Gui, X. C.; Wei, J. Q.; Wang, K. L.; Cao, A. Y.; Zhu, H. W.; Jia, Y.; Shu, Q. K.; Wu, D. H. Carbon Nanotube Sponges. *Adv. Mater.* **2010**, *22*, 617−621.
(34) Gui, X. C.; Zeng, Z. P.; Lin, Z. Q.; Gan, Q. M.; Xiang, R.; Zhu, Y.; Cao, A. Y.; Tang, Z. K. Magnetic and Highly Recyclable Macroporous Carbon Nanotubes for Spilled Oil Sorption and Separation. *ACS Appl. Mater. Interfaces* **2013**, *5*, 5845−5850.
(35) Chen, Z. P.; Ren, W. C.; Gao, L. B.; Liu, B. L.; Pei, S. F.; Cheng, H. M. Three-dimensional flexible and conductive interconnected graphene networks grown by chemical vapour deposition. *Nat. Mater.* **2011**, *10*, 424−428.
(36) Tang, Y.; Gong, S.; Chen, Y.; Yap, L. W.; Cheng, W. l. Manufacturable Conducting Rubber Ambers and Stretchable Conductors from Copper Nanowire Aerogel Monoliths. *ACS Nano* **2014**, *8*, 5707−5714.
(37) Zhang, Y.; Zhu, P. L.; Chen, L.; Li, G.; Zhou, F. R.; Lu, D. Q.; Sun, R.; Zhou, F.; Wong, C. P. Hierarchically Architectures of Monodisperse Porous Cu Microspheres: Synthesis, Growth Mechanism, High-Efficiency and Recyclable Catalytic Performance. *J. Mater. Chem. A* **2014**, *2*, 11966−11973.
(38) Zhang, P.; Shao, C. L.; Zhang, Z. Y.; Zhang, M. Y.; Mu, J. B.; Guo, Z. C.; Liu, Y. C. In Situ Assembly of Well-Dispersed Ag Nanoparticles (Ag NPs) on Electrospun Carbon Nanofibers (CNFs) for Catalytic Reduction of 4-Nitrophenol. *Nanoscale* **2011**, *3*, 3357−3363.
(39) Gao, Y. J.; Zhao, S. F.; Zhang, G. P.; Deng, L. B.; Li, J. H.; Sun, R.; Li, L. Y.; Wong, C. P. In situ assembly of dispersed Ag nanoparticles on hierarchically porous organosilica microspheres for controllable reduction of 4-nitrophenol. *J. Mater. Sci.* **2015**, *50*, 3399−3408.

DOI: 10.1021/acsami.5b00116
ACS Appl. Mater. Interfaces 2015, 7, 6716−6723